Dalton Transactions

Accepted Manuscript

ROYAL SOCIETY OF CHEMISTRY

www.rsc.org/dalton

Energy transfer dynamics and luminescence properties of Eu^{3+} in $CaMoO_4$ and $SrMoO_4$

Santosh K. Gupta[1*], M. Sahu[2], P.S. Ghosh[3], Deepak Tyagi[4], M.K. Saxena[2], R.M. Kadam[1]

[1]Radiochemistry Division, [2]Radioanalytical Chemistry Division, [3]Materials Science Division, [4]Chemistry Division

Bhabha Atomic Research Centre, Mumbai-400085

*Corresponding Author- santufrnd@gmail.com

Telephone- +91-22-25590636

Fax- +91-22-25505151

Abstract:

Undoped and Europium doped $CaMoO_4$ and $SrMoO_4$ scheelite are synthesized using complex polymerization method. Phase purity of the sample is confirmed using powder X-ray diffraction (PXRD). X-ray photoelectron spectroscopy (XPS) was carried out to confirm the oxidation state of various constituent and dopant elements and also presence of oxygen vacancy. Interestingly both $CaMoO_4$ and $SrMoO_4$ on irradiating with UV light give blue and green emission respectively. On europium doping; it was found that molybdate to Eu^{3+} ion energy transfer is more efficient in SrMoO4:Eu compared to $CaMoO_4$:Eu. It is also justified using luminescence lifetime study which shows biexponential decay in case of $CaMoO_4$:Eu corresponding to both host and europium ion; whereas single lifetime is observed in case of $SrMoO_4$:Eu. Anomaly in host-dopant energy transfer is suitably explained using density function theory (DFT) calculations and XPS at Mo edge. The actual site symmetry for europium ion in $CaMoO_4$ and $SrMoO_4$ was also evaluated based on stark splitting pattern which comes out to be D_2 and C_{2v} respectively although it is S_4 for Ca/Ba^{2+} in $AMoO_4$.This is also reflected in higher Ω_2 values for $SrMoO_4$:Eu than $CaMoO_4$:Eu.

1. INTRODUCTION:

Metal Molybdates forms an important class of functional materials which finds application in all areas of science and technology. They belong to the Scheelite structured family with C_{4h} symmetry having two formula units per unit cell. In this particular crystal structure; molybdate ions are loosely connected to metal ions having space group (S.G) $I4_1/a$. Among molybdates; alkaline earth based molybdates systems are much more important functional materials because of their unique structural property and diverse application in various technologically relevant areas. Calcium and strontium molybdate ($CaMoO_4$ and $SrMoO_4$) in particular has been explored for various applications like luminescence host **[1-3]**, biomedical application **[2, 4]**, catalysis **[5, 6]**, energy storage **[7]**, white LED application **[8, 9]** etc. Lanthanide ion-doped inorganic materials is explored extensively owing to their exciting optical properties due to their unique f-f transition, which are unperturbed by the local surrounding leading to a narrow emission peak with high spectral purity. In particular its narrow emission characteristic has been employed to the maximum extent in the field of solid

state lighting like in lamps, field emission displays (FEDs), plasma display panels (PDPs), liquid crystal displays (LCDs), and light-emitting diodes (LEDs).

Among LEDs White light is in huge demand because of its advantageous properties like (i) it is environmentally benign (ii) consumes low power (iii) operation time is long (iv) High brightness [10]. Doping rare earth ion in a suitable host is an efficient way of synthesizing desired phosphor material which is mostly based on f-f or f-d transition of lanthanide ion.

Different rare earth depending upon their energy level; emits in different region and one can tune the color output depending upon the need and applications. However, self activated host emission without doping any activator ion (generally lanthanide) does takes place in various materials, and they transfer their excitation energy efficiently when certain lanthanide or for that say any activator ion is doped in that particular host [11].

Therefore, host to lanthanide ion energy transfer has becomes an efficient route to enhance the photoluminescence intensity of dopant ion.

A europium (Eu^{3+}) ion is the most preferred lanthanide dopant which can be excited by ultra violet (UV) light and is used extensively for phosphor applications. It is considered as a special ion because of (a) non-degenerate $^7F_0$ ground level and non-overlapping $^{2S+1}L_J$ multiplets (b) emission from $^5D_0$ level is the most intense one which is not split into sublevels due to crystal field and (c) in a crystal site with centre of inversion the electric dipole transition (EDT) are strictly forbidden and the magnetic dipole transition (MDT) is usually the most intense and in a site without centre of inversion EDT is usually the strongest emission line, because transition $\Delta J = \pm 2$ are hypersensitive to small deviation from inversion symmetry. Eu^{3+} is most preferred structural probe and is used extensively in for getting information about local symmetry, site occupancy etc. [12-18]. $CaMoO_4$ and $SrMoO_4$ are considered highly suitable luminescence host because of their desired properties like, low phonon energy, wide band gap, structural and thermal stability and easy to synthesize. Among the scheelite-structured molybdate family; $CaMoO_4$ is a self activated luminescence material which emits in the blue and green regions and also in some cases it emits an orange color [19]. It is also reported that $SrMoO_4$ also emits in green region when irradiated with UV light [20]. In literature there is no dearth of luminescence study on Eu^{3+} doped $CaMoO_4$ as well as $SrMoO_4$. Liu and Zhang et al has investigated the effect of charge compensator on photoluminescence (PL) properties of $CaMoO_4:Eu^{3+}$ [21, 22] whereas Hazra and Group demonstrated the PL properties of Ln^{3+}-doped $CaMoO_4$ nanocrystals ($Ln^{3+} = Eu^{3+}$, Er^{3+}/Yb^{3+}) and explore them for bio-imaging and photocatalysis [5]. Eu^{3+} doped $CaMoO_4$ [23, 24] and

$SrMoO_4$ [9, 25] has also been explored extensively for white light technology which is an ever demanding field.

On the other hand Singh et al has investigated the optical and structural property of $CaMoO_4:Eu^{3+}$ on Gd co-doping [1, 26]. Some other work done is related to PL properties of (i) One-dimensional $CaMoO_4:Ln^{3+}$ (Ln=Eu, Tb, and Dy) nanofibers [27], (ii) Eu^{3+} and Sm^{3+} co-doped micro/nanosized $MMoO_4$ (M = Ca, Ba, and Sr) phosphors [28] and (iii) as a function of Bi^{3+} and Eu^{3+} concentrations are studied [29]. Eu doped $SrMoO_4$ has also been studied for their PL properties [9, 30].

But none of them has systematically studied the two systems together and try to understand the difference in photophysical properties of europium in these two molybdates. We have tried to figure out why host to dopant energy transfer is inefficient in calcium molybdate compare to strontium molybdate although there is not much difference in the nature of two hosts, level of doping, synthesis condition etc. using theoretical simulation of experimental data. We have also evaluated the point symmetry of europium ion in two hosts, Judd-Ofelt parameter and other photophysical properties like radiative rate, efficiency, non-radiative lifetime and other related properties in these two hosts and try to evaluate the differences.

2. Experimental details

2.1. Synthesis and Instrumentation:

$Sr_{1-x}Eu_xMoO_4$(s) (x =0, 0.01) and $Ca_{1-x}Eu_xMoO_4$(s) (x =0, 0.01) were prepared by complex polymerization method [31]. The starting materials used were $SrCO_3$(s) (99.99%, M/s Alfa Aesar, Lancaster), $CaCO_3$(s) (99.99%, M/s Alfa Aesar, Lancaster), Eu_2O_3 (99.95% purity supplied by Rare Earth Development Section, BARC, Mumbai), MoO_3(s) (99.5%, Mallinckrodt chemical works, New York), Citric acid (99.7%, M/s Chemco fine chemicals, Mumbai), ethylene glycol (99.0%, M/s Thomas Baker, Mumbai), Selectipur HNO_3 (M/s Merck Ltd, Mumbai) and NH_3 solution (M/s Chemco fine chemicals, Mumbai). $SrCO_3$(s) and $CaCO_3$(s) were preheated at 1123 K for 8 hrs, MoO_3(s) was preheated at 573 K for 4 hrs in air and Eu_2O_3 was preheated at 1273 K for 12 hrs in high purity argon atmosphere before taking the compounds as reactants for the synthesis of $Ba_{1-x}Eu_xMoO_4$(s) (x =0, 0.01) and $Ca_{1-x}Eu_xMoO_4$(s) (x =0, 0.01). For preparation of $Sr_{1-x}Eu_xMoO_4$(s) (x =0, 0.01), the required amount of MoO_3(s) and citric acid was added to distilled water, which resulted in turbid solution and was stirred at 333-353 K for 2-3 hour. Then the required amount of $SrCO_3$(s) was dissolved in dil. HNO_3. The strontium and molybdenum citrate solution was mixed

thoroughly and kept on magnetic stirrer for 1 hour. The citric acid to metal ratio was maintained as 1:1.The pH of the solution was adjusted to 6.5 using ammonia solution which resulted in a transparent and homogeneous solution. After homogenization ethylene glycol was added upon constant stirring for stabilizing the metal ions in polymeric matrix of polyesters. The temperature of the solution was maintained in the range 333-353 K till the formation of a transparent gel. No visible phase separation was observed. The citric acid and ethylene glycol were added in the mass ratio of 6:4. Then the temperature of reaction vessels was raised to 673 K. Combustion of the mixtures took place which resulted in the formations of porous carbonaceous powder which was kept at 773 K for 2 hrs in the furnace. Later the powders were recovered, ground, mixed and pelletised. The pellets were calcined separately at 1123 K for 6 h in air. For the Eu^{3+} doped sample, Eu_2O_3 was dissolved in conc HNO_3 and mixed with molybdenum citrate solution.

Similar procedure were followed for synthesis of $Ca_{1-x}Eu_xMoO_4$(s) (x =0, 0.01), where $CaCO_3$ was taken instead of $SrCO_3$.

X-ray diffraction (XRD) patterns of the powdered undoped and europium doped $LaPO_4$ samples were recorded using RIGAKU Miniflex-600 diffractometer operating in the Bragg-Brentano focusing geometry. Cu-Kα radiation source (λ= 1.5406Å) has been used as X-ray source. Operating voltage and current of the instrument was kept at 40 kV and 30 mA respectively. The XRD patterns were collected with scan rate of 1°/minute. PL data were recorded on an Edinburgh CD-920 unit equipped with M 300 monochromators. The data acquisition and analysis were done by F-900 software provided by Edinburgh Analytical Instruments, UK. A Xenon flash lamp with frequency range of 10–100 Hz was used as the excitation source. Emission spectra for a particular sample was recorded with a lamp frequency of 100 Hz. Multiple Scans (at least five) were taken to minimize the fluctuations in peak intensity and maximize S/N ratio. Fluorescence lifetime measurements were based on well established Time-correlated single-photon counting (TCSPC) technique.

2.2. Computational Methodology:

All calculations in this study are based on density functional theory (DFT) in conjunction with projector augmented wave (PAW) potentials, which is implemented in the plane wave based Vienna Ab-initio Simulation Package (VASP) **[32, 33]**. The generalized gradient approximation (GGA) parameterized by Perdew-Burke-Ernzerhof (PBE) **[34]** was used as the exchange-correlation functional. The projector augmented wave (PAW) potentials **[35]** were used for the ion-electron interactions including the valence states of Ca (3s, 3p, 4s – 10

valence electrons), Sr (4s, 4p, 5s – 10 valence electrons), Mo (4p, 5s, 4d - 14 valence electrons), Eu^{3+} (5p, 6s, 5d - 9 valence electrons) and O (2s, 2p – 6 valence electrons). In our calculations, the Kohn-Sham single particle wave functions were expanded in a plane wave basis with kinetic energy cutoff 500 eV and it shown that the results were well converged at this cut off. For tetragonal $AMoO_4$ (A = Ca and Sr) structure, optimization was carried out with respect to plane wave cut-off energy and k-point meshes to ensure convergence of total energy to within a precision 0.1 meV/atom. In order to study Eu^{3+} doped system, a 2x2x1 supercell of $AMoO_4$ unitcell containing 96 atoms was made. The Brillouin-zone (BZ) integrations were performed on an optimized Monkhorst-Pack **[36]** k-point grid of 16x16x8 for $AMoO_4$ unitcell and 8x8x8 for 2x2x1 supercell. The total energy of $AMoO_4$ and Eu^{3+} doped $AMoO_4$ were optimized with respect to volume (or lattice parameter and c/a ratio), angle and atomic positions. The structural relaxations (b/a, c/a ratio and atomic positions) were performed for each structure using the conjugate gradient algorithm until the residual forces and stress in the equilibrium geometry were of the order of 0.005 eV/Å and 0.01GPa, respectively. The final calculation of total electronic energy and density of states (DOS) were performed using the tetrahedron method with Blöchl corrections **[37]**.

3. Results and discussion:

3.1 X-ray diffraction:

Undoped and $CaMoO_4$:Eu^{3+} samples prepared by complex polymerization route were characterized by x-ray diffraction (XRD) for its phase purity. **Figure 1a** shows the XRD pattern of $CaMoO_4$ and $CaMoO_4$:Eu^{3+} (1.0 mol %). It can be seen from the figure that all diffraction peaks can be indexed to pure tetragonal phase of $CaMoO_4$ and matches well with ICDD card No-29-0351. The XRD pattern of europium doped sample also completely matches with that of blank sample and as such there are no traces of impurity peak. This indicates the formation of pure tetragonal phase for both the molybdate sample; indicating that doping of europium ion has not altered the crystal structure of CaMoO4 and it does occupies the lattice position.

Figure 1b shows the XRD pattern of $SrMoO_4$ and $SrMoO_4$:Eu^{3+} (1.0 mol %). For $SrMoO_4$, all the diffraction peaks matches with the ICDD card No-08-0482 indicating the formation of pure tetragonal phase of $SrMoO_4$ without any traces of impurity. Eu^{3+} doped sample also does not changes much in terms of its diffraction pattern compared to blank sample. This shows that smaller sized Eu^{3+} (106 pm) has been incorporated in the large sized the Sr^{2+} site (126 pm) easily and the doping has not distorted the crystal structure.

The $AMoO_4$ crystal is scheelite structured and the unit cell lattice parameters being a = b = 5.285 Å and c = 11.561 Å for $CaMoO_4$ as well as a = b = 5.466 Å and c = 12.181 Å for $SrMoO_4$ as shown in **Figure 2**. Its space group is $I4_1/a$ (space gr. no. 88) and symmetry point group is S_4. Each Mo ion Mo^{6+} is surrounded by four oxygen ions O^{2-} at a bond length of 1.79 Å and each A ion A^{2+} is surrounded by 8 oxygen ions O^{2-}. Polyhedral of four Mo ions Mo^{6+} surrounding O^{2-} are slightly distorted tetrahedra with angle of O-Mo-O being 107.2, 114.1 and 107.6, 113.2 for $CaMoO_4$ and $SrMoO_4$, respectively. A-O bond length is 2.49 and 2.64 Å for $CaMoO_4$ and $SrMoO_4$, respectively. The DFT-GGA calculated lattice parameters are matching within 1.5 % of the experimentally determined values for both the molybdates. Moreover, the DFT optimized atomic positions are matching within 4 % of the experimentally determined positions. All the experimental and calculated parameters related to $CaMoO_4$ and $SrMoO_4$ are mentioned in **Table 1**.

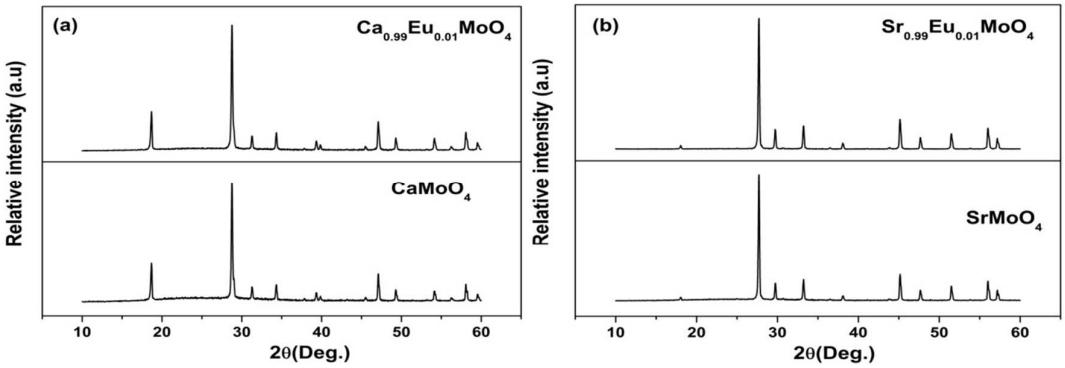

Figure 1: XRD patterns for undoped and 1.0 mol% of Eu^{3+} doped (a) $CaMoO_4$ and (b) $SrMoO_4$ samples

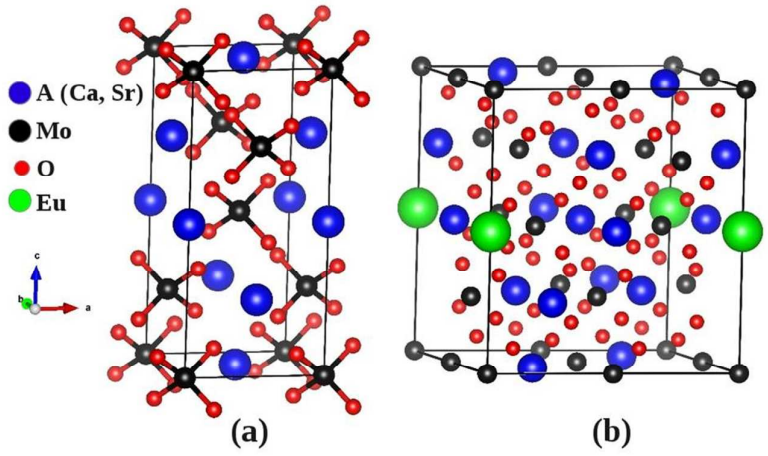

Figure 2: Crystal structure of Undoped and Eu^{3+} doped $AMoO_4$ (A=Ca and Sr)

Table 1: Structural parameter of $CaMoO_4$(s) and $SrMoO_4$(s)

Property	$CaMoO_4$		$SrMoO_4$	
	Calculated	Experiment [38]	Calculated	Experiment [39]
a (Å)	5.285	5.222	5.466	5.380(5)
c (Å)	2.187	2.188	2.228	12.019(9)
Atomic Positions	(4b) 0, 0, 0.5 (4a) 0, 0, 0 (16f) 0.243, 0.147, 0.084	(16f) 0.243 0.101, 0.041	(4b) 0, 0, 0.5 (4a) 0, 0, 0 (16f) 0.238, 0.134, 0.081	(16f) 0.248 0.110 0.051
Volume ($Å^3$)	322.87		363.99	
O-Mo-O angle	107.190, 114.135		107.612, 113.256	
A-O bond length (Å)	2.49		2.64	
Mo-O bond length (Å)	1.79		1.79	

3.2. XPS Study:

XPS is a very sensitive technique for determining the oxidation state of the constituent elements present in molybdate sample. The XPS spectra of Ca and Sr core binding energy (BE) in undoped and europium doped $CaMoO_4$ and $SrMoO_4$ is shown in **Figure 3a** and **3b** respectively. Figure 3a represents XPS peak corresponding to Ca (2p) with core BE of 347.21 eV for $2p_{3/2}$ and 350.67 eV for $2p_{1/2}$.The full width at half maxima (FWHM) of these peaks are 1.9 and 2.2 eV respectively for $2p_{3/2}$ and $2p_{1/2}$. On doping europium ion there is slight shift in binding energy value to lower side. But the intensity ratio; which is represented by I_{Ca} (=BE-$2p_{3/2}$ /BE-$2p_{1/2}$) is found to be 1.67 for undoped and 1.73 for europium doped sample. Also the FWHM values for $2p_{3/2}$ and $2p_{1/2}$ peak in undoped and doped samples doesn't changes significantly. Based on above results it is inferred that calcium stabilizes in +2 oxidation state in both the sample.

Figure 3b represents XPS peak corresponding to Sr (3p) with core BE of 267.89 eV for $3p_{3/2}$ and 278.23 eV for $3p_{1/2}$.The full width at half maxima (FWHM) of these peaks are 3.1 and 2.8 eV respectively for $3p_{3/2}$ and $3p_{1/2}$. It is interesting to note that in case of $SrMoO_4$; on doping europium ion there is slight shift in binding energy value to higher side. But I_{Sr} is found to be 2.29 for undoped and 2.47 for europium doped sample which is within the limit of error bars. There is also not much change in the FWHM values for $3p_{3/2}$ and $3p_{1/2}$ peak in

undoped and doped samples. Based on above results it is inferred that strontium also stabilizes in +2 oxidation states in both undoped and europium doped sample. **Figure S1 (ESI †)** represents XPS peak corresponding to Sr (3d) with core BE of 133.53 eV for $3d_{5/2}$ and 131.97 eV for $3d_{3/2}$.

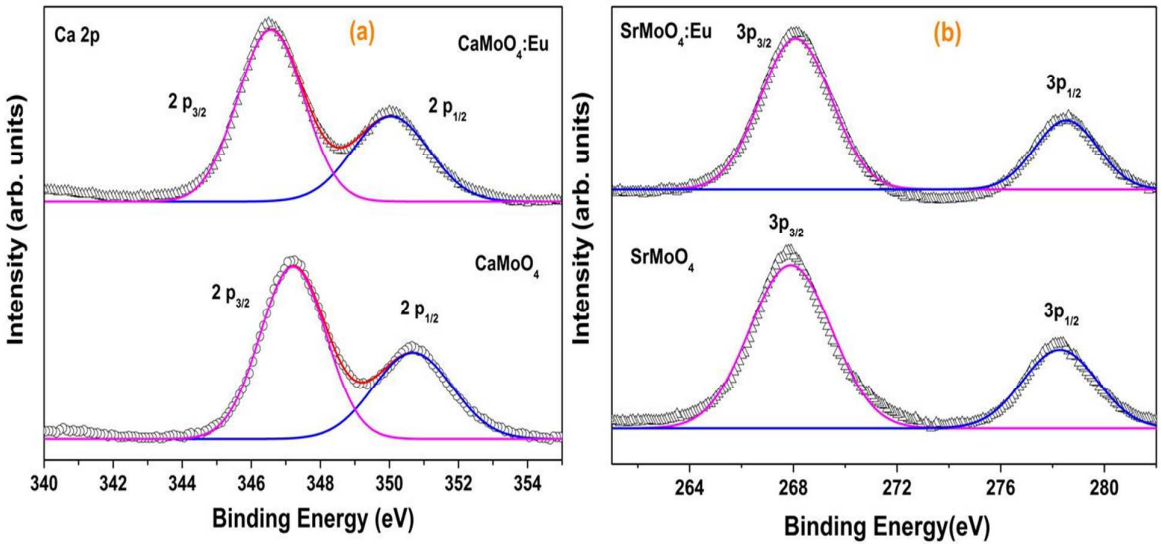

Figure 3: XPS spectra of undoped and europium doped (a) $CaMoO_4$ and (b) $SrMoO_4$. Peaks represents the core binding energy of Ca and Sr.

Figure 4 shows the XPS spectra of the Mo 3d region for molybdenum in undoped and europium doped $CaMoO_4$ and $SrMoO_4$. The peaks nearby 232.6 and 235.7 eV, characteristic of MoO_3, can be attributed to Mo^{6+} $3d_{5/2}$ and $3d_{3/2}$, respectively **[40]**.

Figure 4a represents XPS peak corresponding to Mo (3d) in $CaMoO_4$ with core BE of 232.64 eV for $3d_{5/2}$ and 235.74 eV for $3d_{3/2}$ with FWHM of 1.6 and 2.1 eV respectively. On doping europium ion there is slight shift in binding energy value to lower energy side. But the I_{Mo} is found to be 1.11 for undoped and 1.15 for europium doped sample. Also the FWHM values for $3d_{5/2}$ and $3d_{3/2}$ peak on europium doping doesn't changes significantly. Based on above results and the BE values it is inferred that Molybdenum stabilizes in +6 oxidation state in both undoped and europium doped $CaMoO_4$.

Figure 4b represents XPS peak corresponding to Mo (3d) in $SrMoO_4$ with core BE of 231.33 eV for $3d_{5/2}$ and 234.43 eV for $3d_{3/2}$ with FWHM of 1.6 and 2.2 eV respectively. In this case on doping europium ion there is slight shift in binding energy value to higher energy side which is opposite to what was observed in case of CaMoO4. Interestingly I_{Mo} is found to be exactly same i.e. 1.08 for both undoped and europium doped sample. Also the FWHM values for $3d_{5/2}$ and $3d_{3/2}$ peak in doped and europium doped sample almost equal.

Although the binding energy values and interpretation of I_{Mo} and FWHM values reflects the stabilization +6 oxidation state in both undoped and europium doped $SrMoO_4$; but it is giving different scenario compared to $CaMoO_4$.

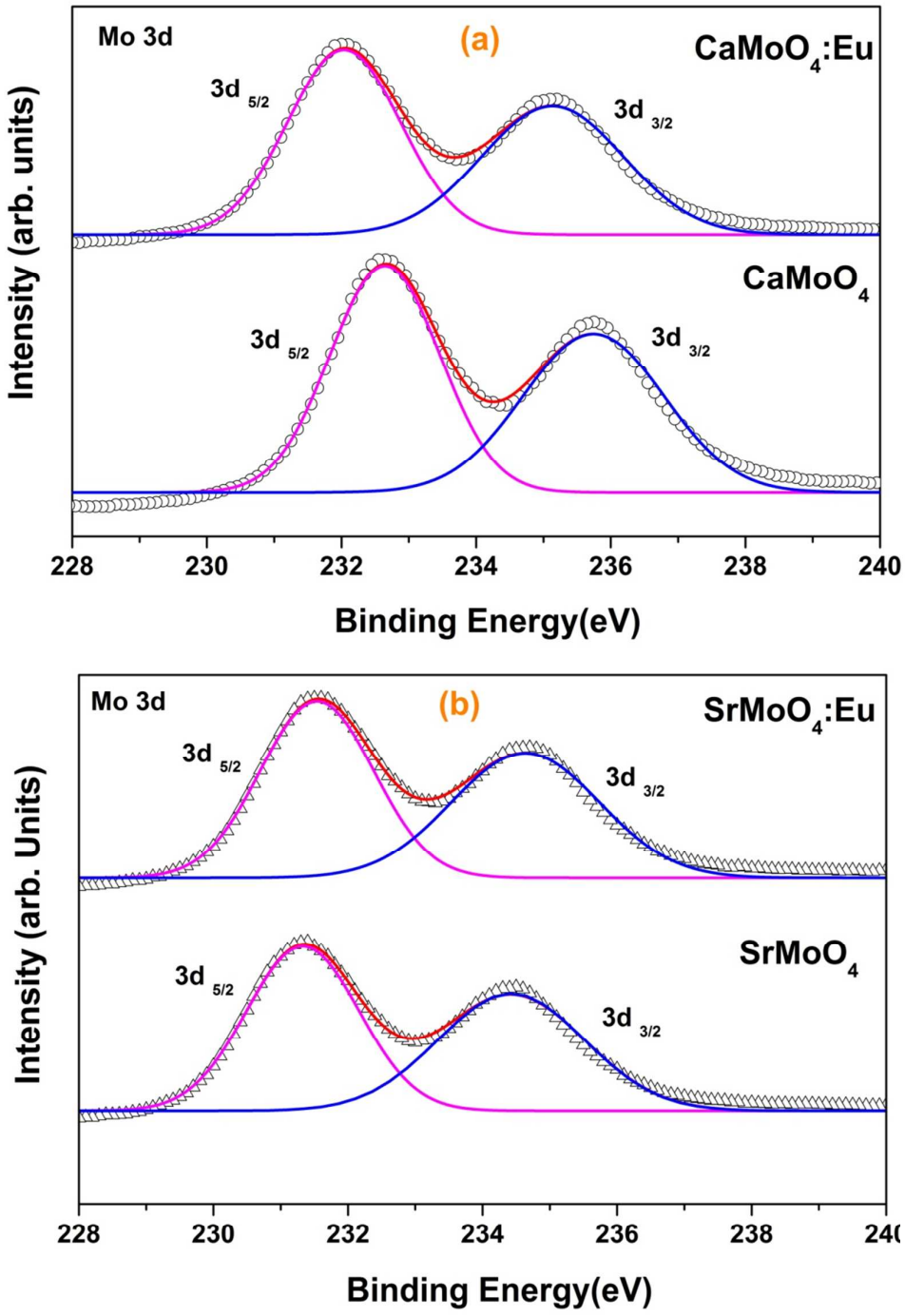

Figure 4: XPS patterns of the Mo 3d region in (a) undoped and $CaMoO_4$:Eu and (b) undoped and $SrMoO_4$:Eu

The XPS spectrum for Eu-3d core level of the $CaMoO_4$:Eu and $SrMoO_4$:Eu samples are shown in **Figure 5** It can be very well seen from the spectrum there are two peaks in the Eu^{3+}

3d region. The peak around 1135 eV in both the samples corresponds to Eu^{3+} $3d_{5/2}$ whereas the peak at 1124 eV is a satellite peak. The BE value for Eu^{3+} $3d_{5/2}$ is in consistent with the reported values for Europium-coordinated ions which indicates that the oxidation states of Europium ions are in +3 for the both the sample [41]. Europium 4d peak is also observed in $CaMoO_4$:Eu sample (**Fig.S2 ESI †**); while in case of $SrMoO_4$:Eu it is not visible because spectral region of Eu 4d coincides with that of Sr 3d.

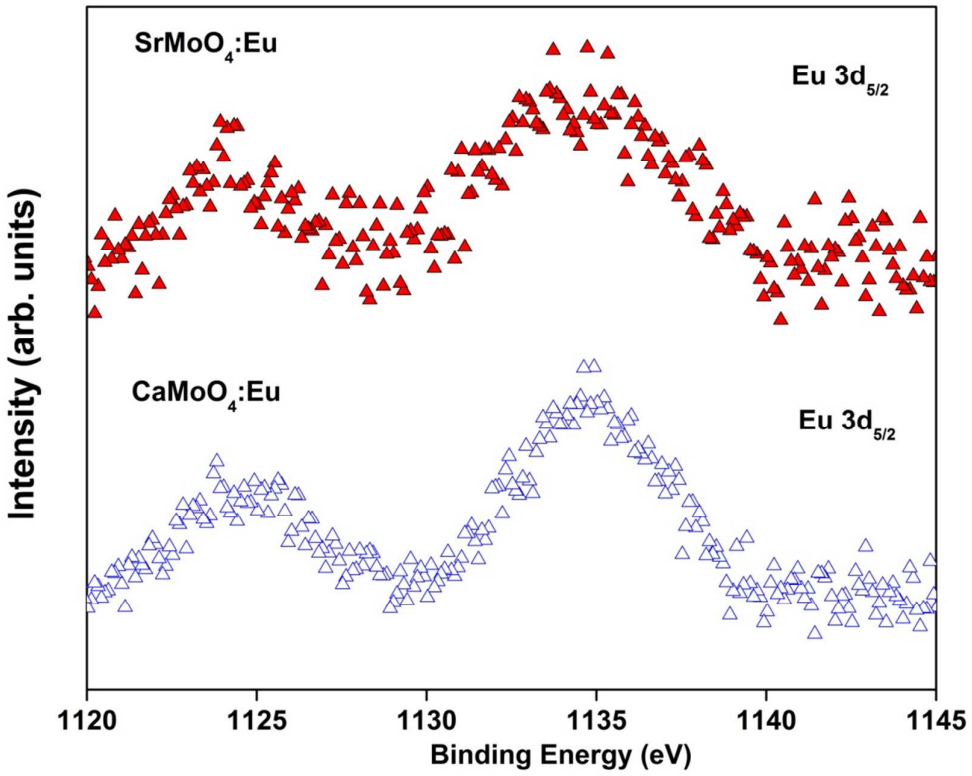

Figure 5: XPS core level spectra of europium 3d level of $CaMoO_4$:Eu and $SrMoO_4$:Eu

Figures 6(a) and (b) depict the O 1s core level peak of the $CaMoO_4$ and $SrMoO_4$ samples. The O 1s core level peak in case of **Fig. 6a** shows a slightly asymmetric peak at ~530 eV and is fitted with two symmetric Gaussian curves represented as O_a and O_b peaks.

The O_a peak is ascribed to lattice oxygen atoms of $CaMoO_4$. There are quite a few reports that indicated high energy peak (O_b) of O 1s arises due to hydroxyl group or chemisorbed oxygen and organic oxygen on the surface of the sample such as CO, COO^- [42, 43].

However, the asymmetric nature of high energy peak (O_b) in an O 1s XPS spectrum is typical of presence of oxygen vacancy in the sample [44].

This fact is also supported by Naeem *et al.* where they have observed that Ob peak is developed with increasing oxygen vacancies [45]. After comparing the integral area ratio of Ob/ Oa in the $CaMoO_4$ and $CaMoO_4:Eu^{3+}$, it is observed that the area ratio of the $CaMoO_4:Eu^{3+}$ is higher than that of $CaMoO_4$ indicating the enhancement of oxygen vacancy concentration. This is consistent with the fact that concentration of defects and oxygen vacancies increases on doping trivalent europium ion at divalent Ca^{2+} site.

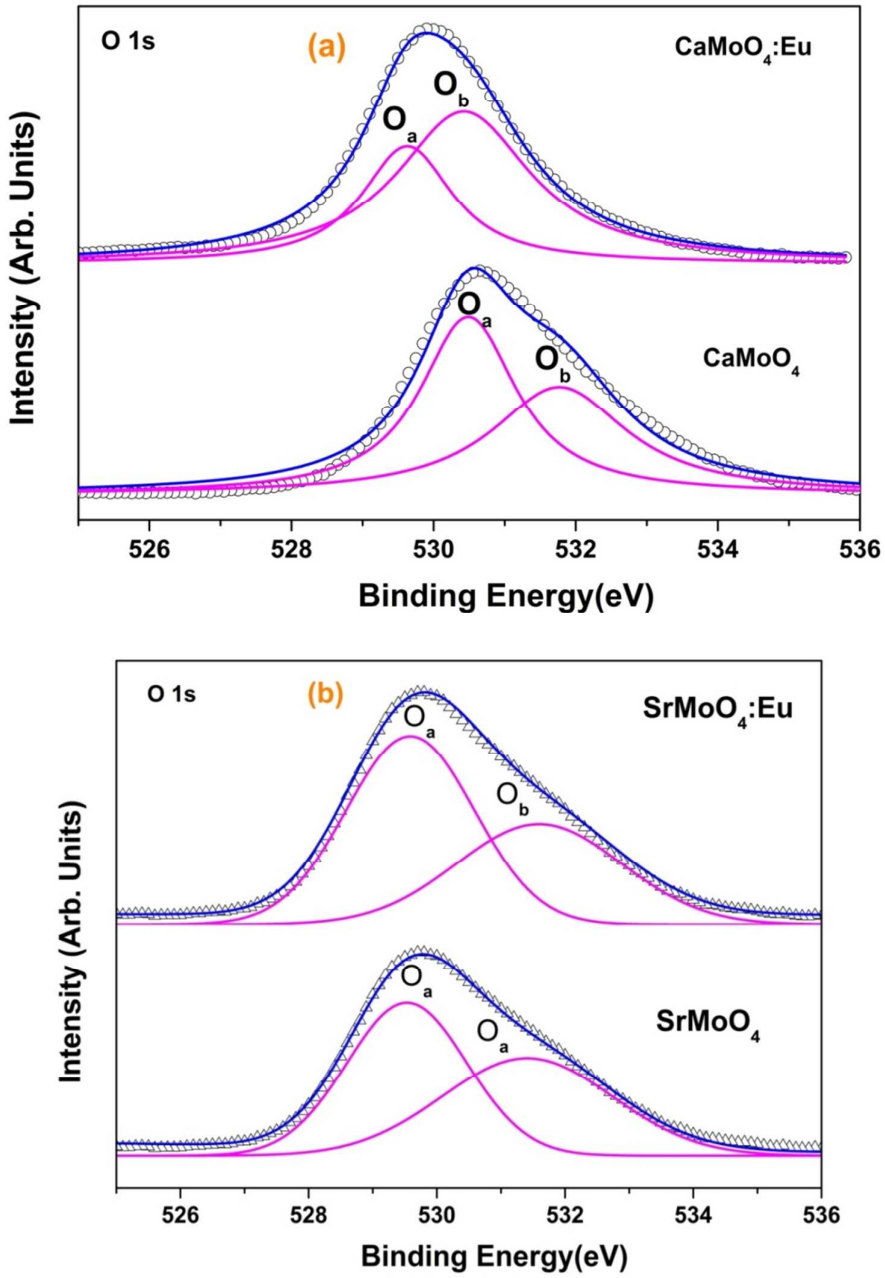

Figure 6: XPS core level spectra of (a) oxygen 1s level of $CaMoO_4$ and (b) oxygen 1s level of $SrMoO_4$

3.3. Emission spectroscopy of $CaMoO_4$ and $SrMoO_4$

Emission spectra of undoped $CaMoO_4$ and $SrMoO_4$ under the excitation wavelength of 250 nm are depicted in **Figure 7**. It can be seen from the figure that emission spectrum of $CaMoO_4$ display a broad band at around 420 nm (blue region) whereas that of $SrMoO_4$ shows a broad band at 540 nm (Green region). Such bluish-green emission in molybdate based compounds is attributed to charge transfer transition within MoO_4^{2-} group **[46]**.

But depending on (i) particle size of the prepared material (2) synthesis methodology (iii) morphology and (iv) presence of oxygen vacancies; the peak maxima differs. Such transitions are normally related to the electron–hole recombination process after excitation using the band gap of O-Mo charge transfer transition in MoO_4 tetrahedra **[48]**.

It is reported that in case of $CaMoO_4$ emission peak maxima normally appears to around 480-510 nm **[46, 47]** but it is blue shifted if the size is nano domain **[48]** due to quantum confinement effect.

There are lots of explanations given in literature related to photoluminescence in undoped $SrMoO_4$. In our sample emission maxima for $SrMoO_4$ is observed at 540 nm which exactly matches with that reported for that $SrMoO_4$ powder obtained by co-precipitation method **[49]**. But there are reports where an emission peak maximum in $SrMoO_4$ differs; depending upon the synthesis methodology like at 485 nm for film produced using galvanic cell method, 520 nm for film synthesized using electrochemical method and at 390 nm for powder sample obtained using microemulsion method **[50-52]**. This difference can be attributed to different levels of structural organization takes place depending upon the synthesis and thermal treatment conditions.

It can also be seen from the **Figure 7** that integral intensity of PL emission for $CaMoO_4$ is much more than that of $SrMoO_4$. This can be correlated with the increase in ionic radius of the given cations in the order $Sr^{2+} > Ca^{2+}$. This phenomenon can be explained in the frames of the configuration curves model, because the shift of the exited state parabola (parabola offset) depends on the cation ionic radius **[53]**. The larger is the cation ionic radius, the greater is the parabola offset value, and, accordingly, the greater is the probability of nonradiative transition from the exited state; and therefore lesser is the radiative transition intensity.

In order to evaluate the colorimetric performance of the material, the color coordinates for the sample $AMoO_4$ were calculated using the intensity-corrected emission spectra excited by 250 nm. The calculated CIE coordinates for $CaMoO_4$ and $SrMoO_4$ is mentioned in the

chromaticity diagram which is shown in **Fig. 3 (ESI †)**. As can be seen from the figure that $CaMoO_4$ and $SrMoO_4$ respectively emits in blue and yellowish green region.

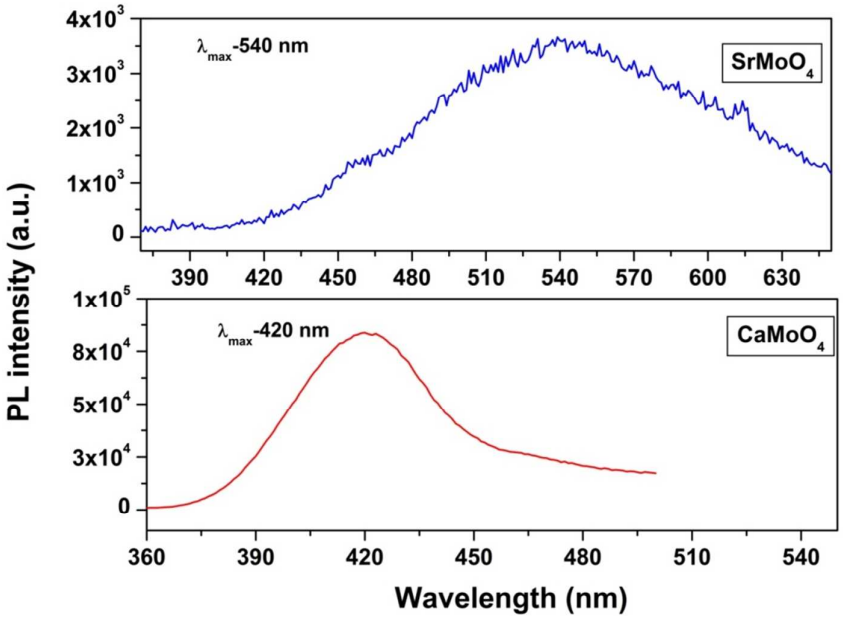

Figure 7: Emission spectra of $CaMoO_4$ and $SrMoO_4$ (λ_{ex}-245 nm).

Figure 8 shows the PL decay curve for $CaMoO_4$ and $SrMoO_4$ sample recorded at 77 K. It can be seen from the figure that both $CaMoO_4$ and $SrMoO_4$ display monoexponential behavior with lifetime value of 41.3 and 27.8 μs. There is close correspondence between emission intensity and PL lifetimes.

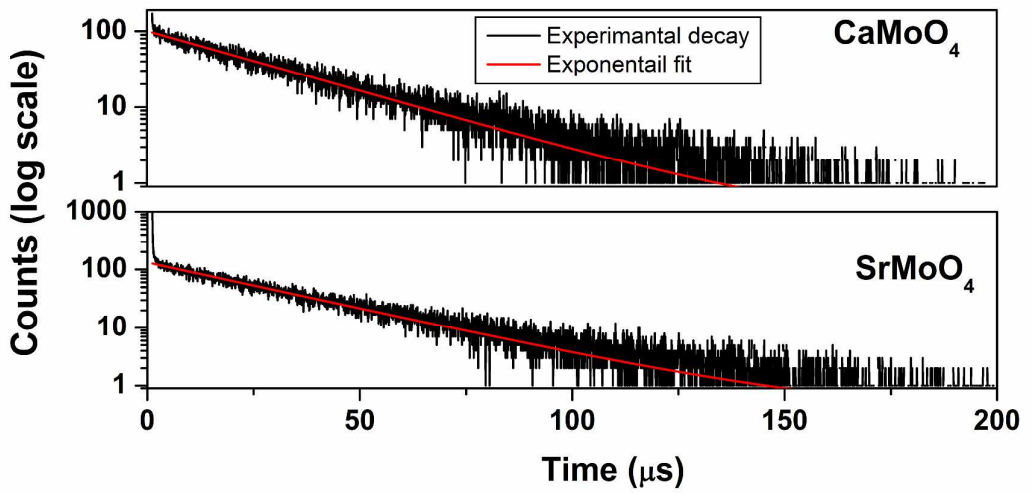

Figure 8: PL decay profile of $CaMoO_4$ and $SrMoO_4$ under excitation wavelength of 250 nm and emission wavelength of 420 and 540 respectively.

3.4. Photoluminescence study of Europium doped $CaMoO_4$ and $SrMoO_4$:

Figure 9 shows the excitation spectra of $CaMoO_4:Eu^{3+}$ and $SrMoO_4:Eu^{3+}$ sample with emission wavelength of 615 nm; corresponding $^5D_0$-$^7F_2$ transition of Eu^{3+} ion. The spectra shows an intense broad band in the spectral range of 240–330 nm and some weak features in the range of 330 –500 nm. The broad band consist of two features; one at 250 nm and the other at 300 nm due to overlap of the charge transfer (CT) transitions of $O^{2-} \rightarrow Mo^{6+}$ and $O^{2-} \rightarrow Eu^{3+}$ groups, and the contribution of the O-Mo CT transition is the dominant one. The weaker peaks above 350 nm are attributed to intra f-f transition of Eu^{3+} ions. Among these; $^7F_0 \rightarrow {}^5L_6$ (395 nm) and $^7F_0 \rightarrow {}^5D_2$ (467 nm) lines are relatively intense one. The interesting observation is O-Eu charge transfer peak in $CaMoO_4$ is slightly red shifted (260 nm) relative to $SrMoO_4$ (250 nm).

It is known that position and intensity of charge transfer band is strongly affected by the extent of covalency in O^{2-}-Ln^{3+} bond. In the structure of Eu^{3+}–O^{2-}—A^{2+} (A = Ca and Sr), the extent of covalency in Eu^{3+}–O^{2-} bond is weaker in $CaMoO_4$-Eu^{3+} because Ca^{2+} ion pulls electrons of O^{2-} ions strongly because of its large electronegativity (1.00 in Pauling electronegativity scale) and smaller ionic size compared to Sr^{2+} (0.95 in Pauling electronegativity scale) in $SrMoO_4$-Eu^{3+}. So, it is easier for the electron from O-2p state to get transferred to Eu 4f state in $SrMoO_4$ host than that in $CaMoO_4$.

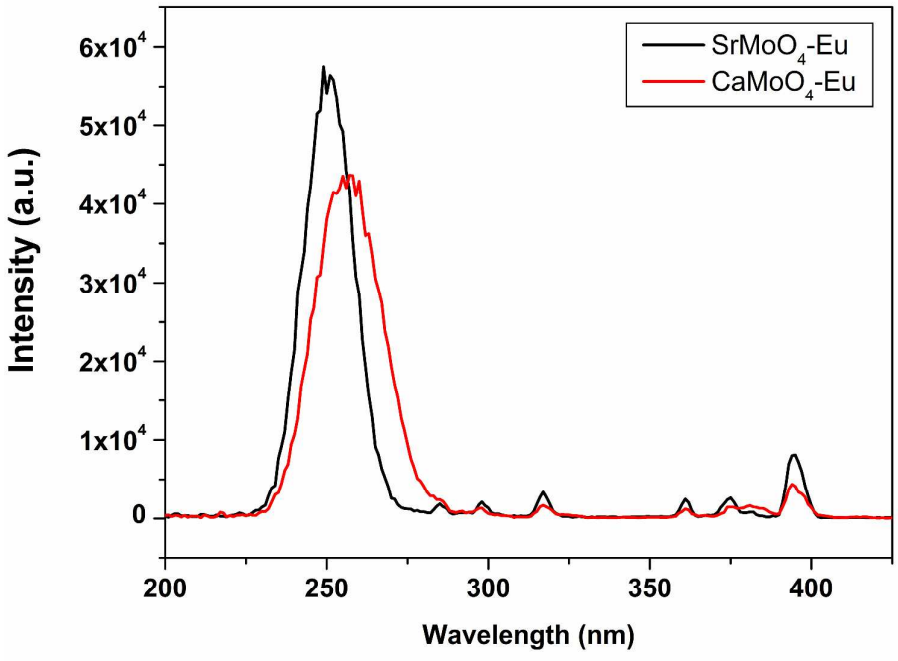

Figure 9: Excitation spectra of the powder sample of Eu^{3+} ion doped $CaMoO_4$ and $SrMoO_4$.

Figure 10 displayed the emission spectra of $CaMoO_4$: Eu^{3+} and $SrMoO_4$: Eu^{3+}. Upon excitation into charge transfer state (CTS) of Eu^{3+}, the emission spectra shows typical features of trivalent europium ion in solids and the peaks are labelled in the spectra itself. The characteristics emission of Eu^{3+} involving ($^5D_0$-^7F_j, J=0-4) can be easily seen from the emission spectra of both $CaMoO_4$ and $SrMoO_4$ sample shown in **Figure 10**. The interesting observation which can be made out from the **Figure 10** is the extent of host-dopant energy transfer; which is relatively much higher in $SrMoO_4$-Eu is than that in the case of $CaMoO_4$-Eu. This is clearly evident from the presence of substantial host emission band along with Eu^{3+} in $CaMoO_4$-Eu emission spectrum. This is very unusual to interpret because dopant ion is same, level of doping is 1.0 % in both the host, and synthesis condition is exactly identical; but still Eu^{3+} display different emission characteristics in $CaMoO_4$ and $SrMoO_4$.

The mechanism of energy transfer from molybdate to Eu^{3+} ion is pictorially depicted in **Fig. 4 (ESI †)**

It is well known that $^5D_0 \rightarrow {}^7F_1$ transition of Eu^{3+} ion at 592 nm is allowed by magnetic dipole transition (MDT) and it is negligibly affected or unaffected by local field surrounding the Eu^{3+} ion, whereas the $^5D_0 \rightarrow {}^7F_2$ Eu^{3+} ion at 615 nm is allowed by electric dipole transition (EDT) and is extremely sensitive to environmental factor such as crystal field or local symmetry in the vicinity of the Eu^{3+} ion. Because of this typical characteristic; $^5D_0 \rightarrow {}^7F_2$ transition of Eu^{3+} is called hypersensitive transition. The ratio of integral intensity of hypersensitive ED transitions ($^5D_0 \rightarrow {}^7F_2$) and MD transition ($^5D_0 \rightarrow {}^7F_1$), which is referred as the asymmetry ratio (I), gives an idea about the extent of structural distortion when trivalent europium ion is doped in any inorganic host. The fact that in both $CaMoO_4$ and $SrMoO_4$; $^5D_0$-$^7F_2$ EDT at 615 nm is much more intense than the magnetic dipole transition ($^5D_0 \rightarrow {}^7F_1$) transition at 592 nm indicates that Eu^{3+} at Ca^{2+}/Sr^{2+} site deviates from inversion symmetry and the local symmetry around europium ion in both these sample is quiet low. The exact local symmetry around Eu at Ca and Sr site is calculated in the next section.

It is reported that in $CaMoO_4$; Ca^{2+} is coordinated with eight oxygen atoms (CaO_8) and has S_4 point symmetry **[54]**. Similarly in $SrMoO_4$ also point symmetry of Sr and Mo is S_4 only **[49]** with 8 and 4 coordination respectively.

When Eu^{3+} is incorporated in $SrMoO_4$ or $CaMoO_4$; based on ionic radii analogy it should occupy Ca^{2+}/Sr^{2+} site. Because of size and charge mismatch Eu^{3+} doping induces significant structural distortion and further reduces the symmetry from S_4 in both $CaMoO_4$ and $SrMoO_4$.

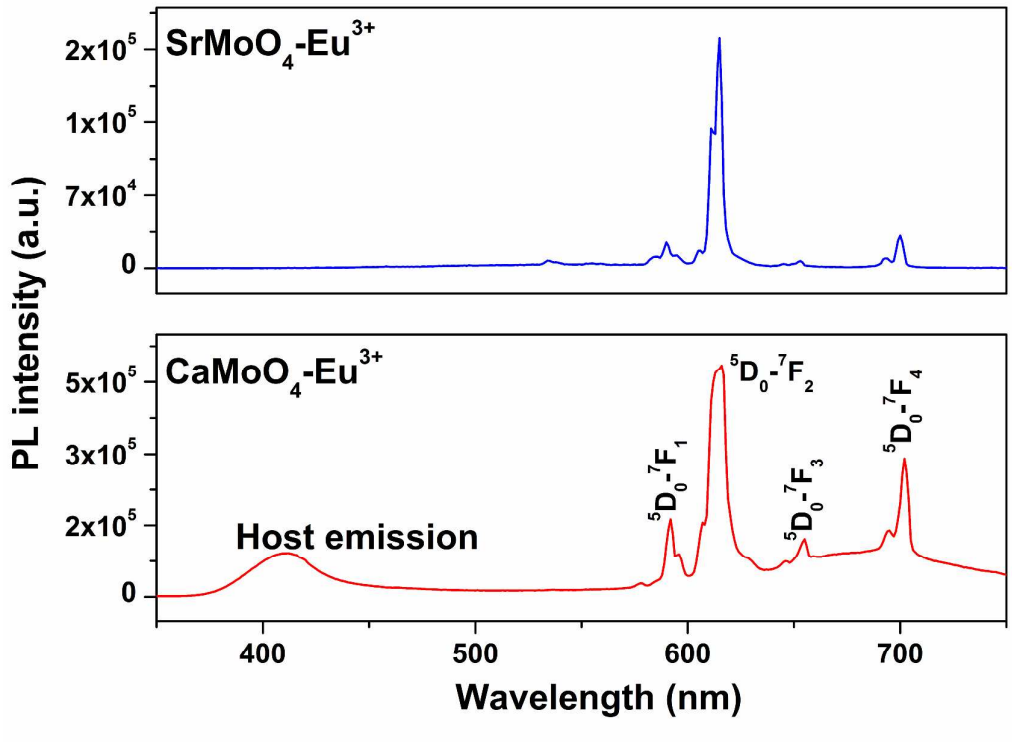

Figure 10: Emission spectra of $CaMoO_4$: Eu^{3+} and SrMoO4: Eu^{3+} under excitation with their respective charge transfer band.

As discusses in the earlier section that in $CaMoO_4$/$SrMoO_4$ the coordination number of Ca/Sr site is 8 and that of Mo site is 4. These are the two cationic sites which can be occupied by the Eu^{3+} ions. But the constraint of ionic size matching allows only europium ion to occupy alkaline earth ion site i.e. Ca^{2+} or Sr^{2+} in $CaMoO_4$ and $SrMoO_4$ respectively. To get an idea about such site occupancy by europium ion we have conducted photoluminescence life time measurements. The decay curves recorded at 77 K corresponding to the $^5D_0$ level of Eu^{3+} ions in the 1.0 mol % Eu^{3+} doped $CaMoO_4$ and $SrMoO_4$ are shown in **Figure 11** under excitation corresponding to charge transfer and emission wavelength of 615 nm. For $CaMoO_4$-Eu, decay curve obeys a biexponential behavior and the fitted equation is mentioned in equation (1).

$$I(t) = A_1 \exp\left(-\frac{t}{\tau_1}\right) + A_2 \exp\left(-\frac{t}{\tau_2}\right) \quad \textbf{(1)}$$

Where I(t) is intensity, τ_1 and τ_2 are emission decay times, and A_1 and A_2 are their relative weightage. The decay curve shows two different lifetime value 35.4 µs (T_1) and 862.8 µs (T_2) with magnitudes 23 and 78 % respectively with average lifetime of 662 µs. This is probably the radiative lifetime because at such low temperature all vibration leading to multiphonon relaxation is quenched. T_1 species is because of host contribution and T_2 is the lifetime of

europium sitting at Ca^{2+} site. The presence of T_1 along with T_2 itself shows that extent of energy transfer from host to Eu^{3+} ion is low. This can also be corroborated with lifetime value of $CaMoO_4$ host in pure form and europium doped sample. The radiative lifetime of blank $CaMoO_4$ sample is 41.3 µs and it has not reduced substantially in doped sample (35.4 µs). This also indicates that inefficient host dopant energy transfer in $CaMoO_4$:Eu^{3+} host compared to $SrMoO_4$:Eu^{3+}.This we have also corroborated with DFT calculations in section 3.5.

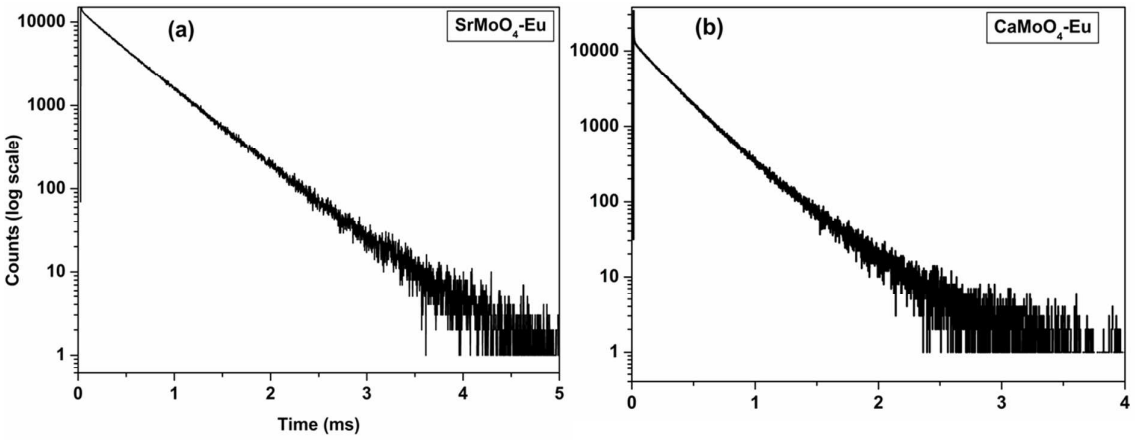

Figure 11: PL decay profile of (a) $SrMoO_4$: Eu^{3+} and (b) $CaMoO_4$: Eu^{3+} under excitation under excitation with their respective charge transfer band and emission wavelength of 615 nm recorded at 77 K.

3.5. Stark splitting patterns in $CaMoO_4$: Eu^{3+} and SrMoO4: Eu^{3+}.

As discussed earlier also that point symmetry of Ca/Sr in $AMoO_4$ scheelite structure is S_4. When Eu^{3+} is doped in $CaMoO_4$/ $SrMoO_4$ host; because of size and charge difference; defects are bound to form. Charge mismatch can cause the formation of cation vacancy whereas size mismatch can cause lattice strain. The overall impact is lowering of symmetry and distorted local environment around europium ion. As a result intense EDT is observed in the emission spectra of $CaMoO_4$ and $SrMoO_4$ doped with Eu^{3+}.

We have tried to examine the number of peaks (called as stark splitting) in the selective emission zone of MDT and hypersensitive EDT plotted in **Figure 12** and tries to derive upon the point symmetry around Eu^{3+}.

It is very well known that (2J + 1)-degenerate J-levels of Eu^{3+} ion is splits into so-called Stark sub-levels by ligand field effect when they are inserted into a chemical/ligand environment, and their number depends on the local site symmetry of the metal ion. ED and

MD forbidden $^5D_0 \rightarrow {}^7F_0$ transition in case of Eu^{3+} is allowed only when symmetry around it is very low namely: C_s, C_1, C_2, C_3, C_4, C_6, C_{2V}, C_{3V}, C_{4V}, and C_{6V}, **[55].** This particular transition is appearing in the emission spectrum of $SrMoO_4$-Eu which confirms the fact; that the site symmetry in this particular case has to be among the one mentioned above.

The substitutions of Sr^{2+} with Eu^{3+} results in significant lattice distortion because of size and charge mismatch. From stark splitting pattern shown in **Figure 12a**, three peaks for $^5D_0 \rightarrow {}^7F_1$ MD transition and four lines for $^5D_0 \rightarrow {}^7F_2$ ED transition of Eu^{3+} were resolved for $SrMoO_4$:Eu^{3+} (1.0 mol %) . According to the branching rules of various point groups **[56, 57],** it infers that the actual site symmetry of Eu^{3+} in $SrMoO_4$ is $\mathbf{C_{2v}}$.

But in case of $CaMoO_4$: Eu^{3+} (**Figure 12b**); $^5D_0 \rightarrow {}^7F_0$ is absent and three peaks for $^5D_0 \rightarrow {}^7F_1$ MD transition and three peaks for $^5D_0 \rightarrow {}^7F_2$ ED transition of Eu^{3+} were resolved. Therefore in this particular case point symmetry of Eu^{3+} is $\mathbf{D_2}$ which is slightly higher than that in case of $SrMoO_4$-Eu. The question is why is it so?

This means that Europium is causing more distortion in $SrMoO_4$ lattice than in $CaMoO_4$ at same level of doping. It can be interpreted in terms of cation radii. The values of ionic radii in Å follow the following trend: [8-Sr^{2+} (1.26) > 8-Ca^{2+} (1.12) ~8-Eu^{3+} (1.07) **[58]**. On the basis of these values it can be inferred that because of close proximity between ionic radius of 8-coordinated Ca^{2+} and 8-coordinated Eu^{3+} than between Eu^{3+} and Sr^{2+} makes; europium occupies Ca site with less strain compared to Eu sitting at Sr site. Therefore its symmetry reduces to lower value in $SrMoO_4$ than in $CaMoO_4$.

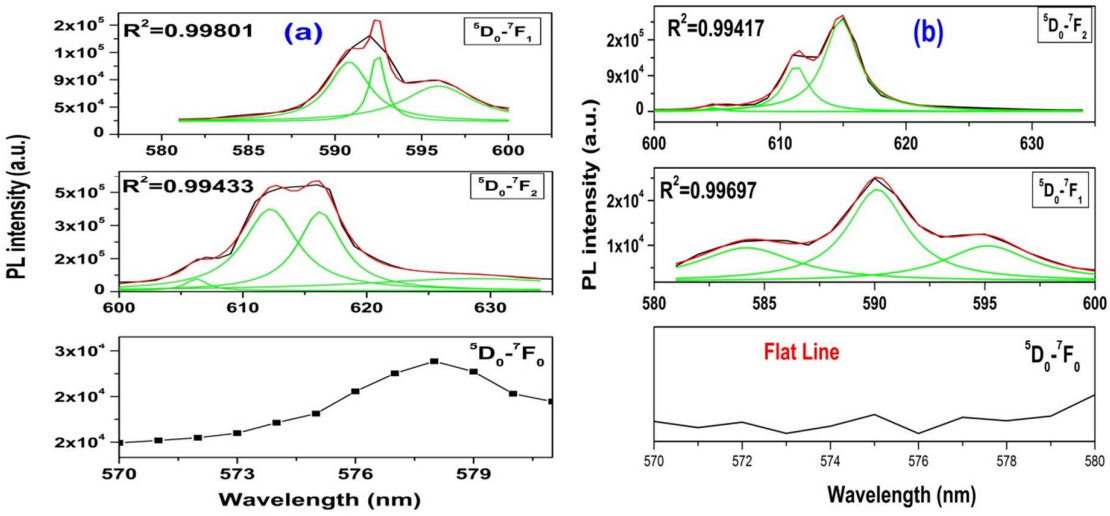

Figure 12: Gaussian fitted fluorescence spectra for selective region in (a) $SrMoO_4$: Eu^{3+} and (b) CaMoO4: Eu^{3+}. Black line is the experimentally observed, red is Gaussian fitted and green indicates the deconvoluted components in each case.

3.6. DFT calculations

The DFT-GGA calculated total and angular momentum projected electronic density of states (DOS) of $CaMoO_4$ and $SrMoO_4$ are presented in **Figure 13**. From **Fig. 13** it can be noted that the conduction band from -5 to 0 eV is formed mainly by the Mo 4d as well as O 2p states in the lower part and A s, p states (A= Ca, Sr) as well as O 2p states in the upper part. Presence of bonding and antibonding states signifies strong hybridization of Mo and O atoms in Mo-O bonds. The d-states of A (Ca, Sr) present mostly and significantly in the conduction band region. A pseudo-gap is present in the middle of the conduction band and width of the pseudo-gap is 0.08 and 0.4 eV for $CaMoO_4$ and $SrMoO_4$, respectively. Presence of pseudo-gap is manifestation of covalent bonding in these molybdates and character of covalent bonding in $SrMoO_4$ is stronger than $CaMoO_4$. It is evident from the figure that the top of the valence band is formed predominantly by *p* states of oxygen with admixture of small A (Ca, Sr) s, p and *d* states. The lower part of the conduction band is mainly d states of Mo and A (Ca, Sr) with small contribution from O p states. The DFT-GGA calculated electronic band-gap of $CaMoO_4$ and $SrMoO_4$ is 2.95 and 3.7 eV, respectively. Experimentally determines band-gap of $CaMoO_4$ is 4.22 **[59]** and 4.5 eV **[60, 61]** and UV–visible absorbance spectra measured (at room temperature) band-gap for the $SrMoO_4$ powders processed in microwave-hydrothermal at 413 K for 5 h is 3.98 eV **[62]**. In both cases DFT-GGA calculated band-gap is underestimated with respect to the experimentally determined values and amount of underestimation is more for the $CaMoO_4$ compared to $SrMoO_4$. Such an underestimation of the band gap is well-known for the different exchange-correlation functions of the DFT calculations.

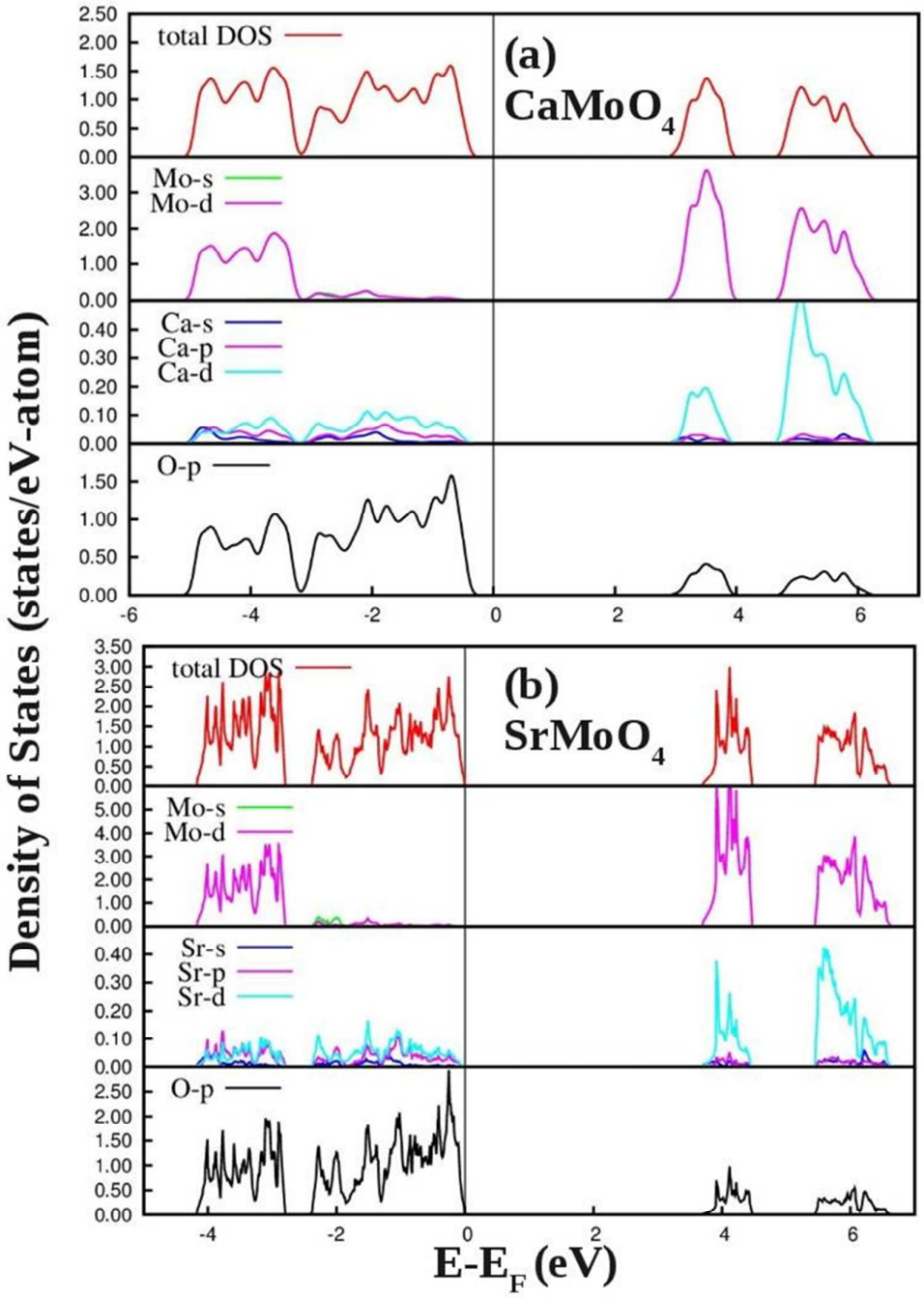

Figure 13: DFT-GGA calculated density of states (DOS) of pure $CaMoO_4$ and $SrMoO_4$. Vertical lines at 0 eV represent Fermi energy (E_F).

The DFT-GGA calculated total and angular momentum projected electronic density of states (DOS) of Eu doped $CaMoO_4$ and $SrMoO_4$ are presented in **Figure 14 and 15** respectively. Overall bonding features are same for $AMoO_4$ and Eu doped $AMoO_4$ (A= Ca, Sr) but some notable differences are present. Due to Eu doping Fermi energy has shifted to bottom of the

conduction band and a small amount of impurity states are present at the Fermi level. DFT-GGA calculated electronic band-gap of Eu^{3+} doped-$CaMoO_4$ and Eu doped-$SrMoO_4$ is 3.35 eV and 3.63 eV, respectively. In these calculations Eu^{3+} ion is doped in the A sub-lattice as ionic radius of Eu^{3+} (in 8 coordination, 1.2 Å) is smaller compared to Ca^{2+} (in 8 coordination, 1.26 Å) and Sr^{2+} (in 8 coordination, 1.4 Å). Eu-O bond length in doped $CaMoO_4$ and doped $SrMoO_4$ is 2.42 and 2.46 Å, respectively. Reduction in bond length of Eu-O compared to the parent A-O bond is higher in doped $SrMoO_4$ compared to $CaMoO_4$. **Figure 14 and 15** clearly shows degree of hybridization of d states of Eu^{+3} and p-states of O is almost similar to Ca^{2+}-O bonding in $CaMoO_4$ but significantly different compared to Sr^{2+}-O bonding in $SrMoO_4$. Presence of sharp peaks in the upper part of Eu partial-DOS of doped $SrMoO_4$ signifies strong d-p bonding. This also manifests Eu^{3+} ions interact strongly with $SrMoO_4$ compared to $CaMoO_4$ hence optical energy transfer from host to dopant atom is favorable in $SrMoO_4$ compared to $CaMoO_4$.

If we go back to our discussion on PL properties of undoped CaMoO4 and SrMoO4; emission in such cases is attributed to O to Mo charge transfer transition within MoO_4^{2-} group. So Mo chemical identity plays in important role in physics involve in Host-dopant energy transfer dynamics.

XPS data also shows that I_{Mo} (=BE-$3d_{5/2}$ /BE-$3d_{3/2}$) for molybdenum changes on europium doping compared to undoped $CaMoO_4$ whereas no such is seen in case of $SrMoO_4$. Interestingly in case of SrMoO4 sample; I_{Mo} is found to be exactly same even on europium doping i.e. 1.08 for both undoped and europium doped sample. Also the FWHM values for $3d_{5/2}$ and $3d_{3/2}$ peak in doped and europium doped sample almost equal.

This can be another probable region why energy transfer from host to Eu doesn't takes place in case of Eu^{3+} doped-$CaMoO_4$ but it is highly efficient in case of Eu^{3+} doped-$SrMoO_4$.

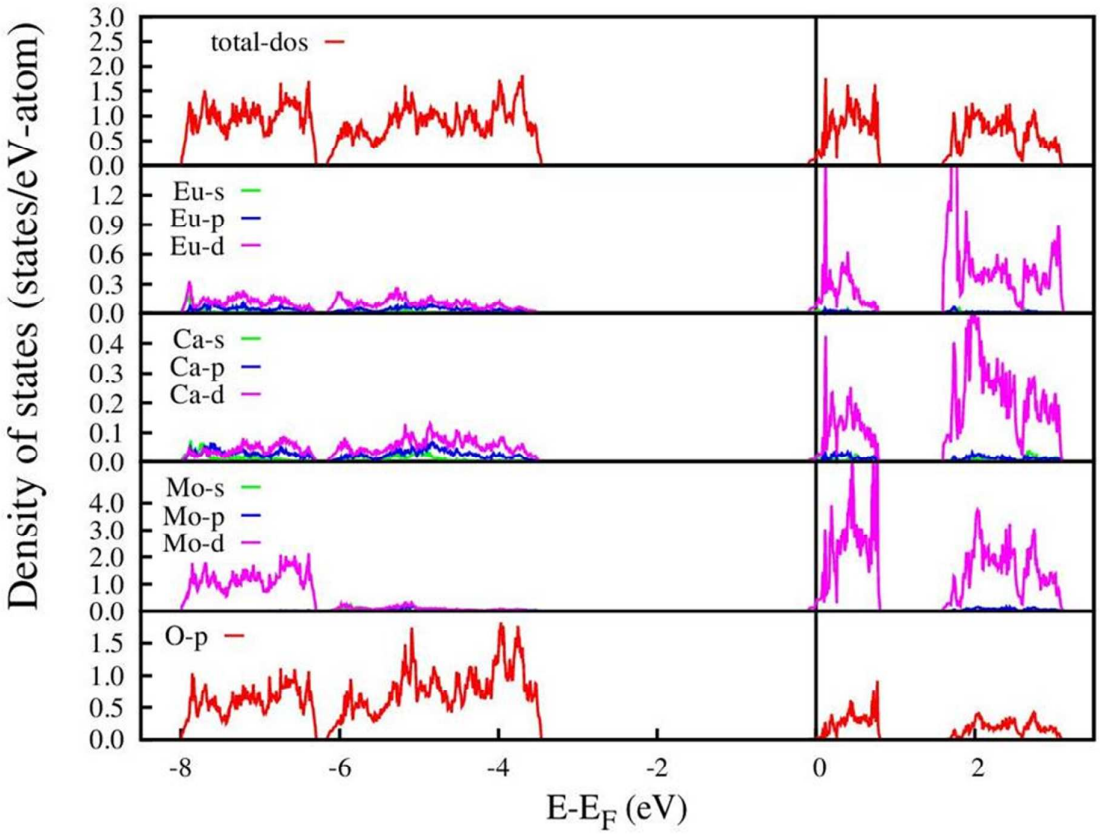

Figure 14: DFT-GGA calculated density of states (DOS) of Eu^{3+} doped $CaMoO_4$. Vertical lines at 0 eV represent Fermi energy (E_F).

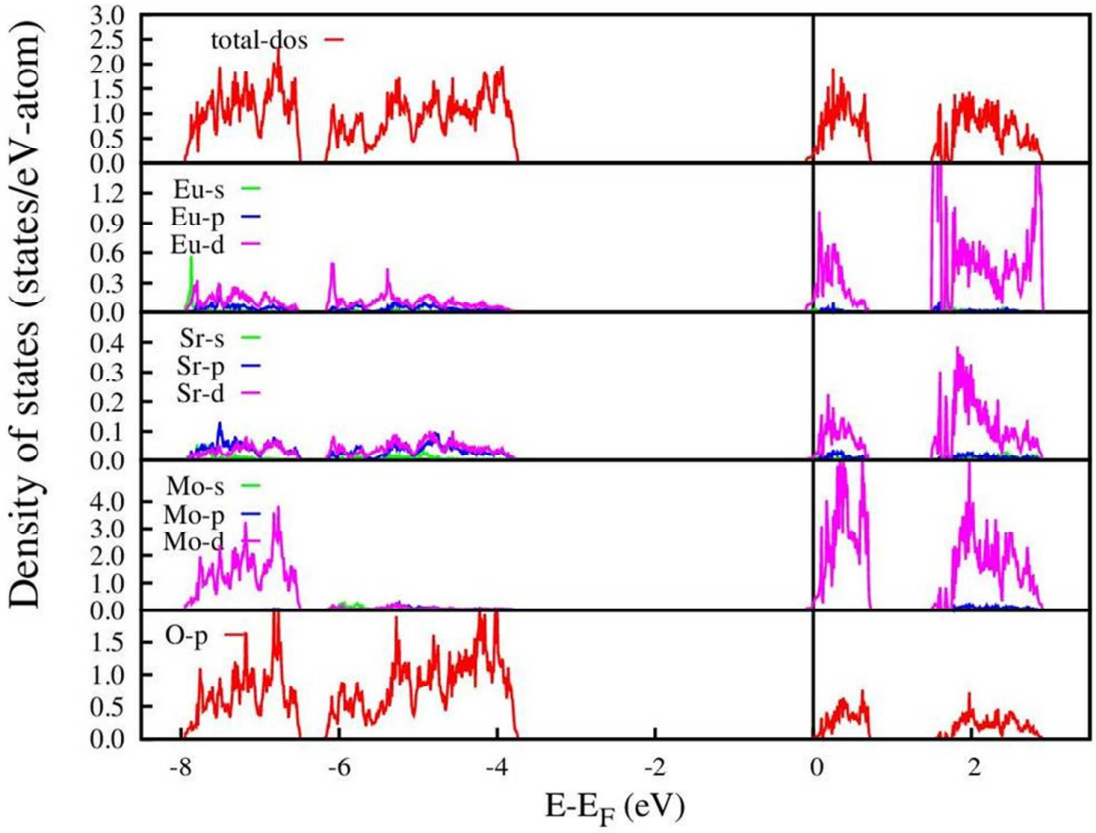

Figure 15: DFT-GGA calculated density of states (DOS) of Eu^{3+} doped $SrMoO_4$. Vertical lines at 0 eV represent Fermi energy (E_F).

3.7. Comparison of photophysical properties of $CaMoO_4$ and $SrMoO_4$ doped Eu- Judd-Ofelt Analysis:

The comparison of EDT and MDT for $CaMoO_4$: Eu^{3+} and SrMoO4: Eu^{3+} in terms of their integral intensity is shown in **Fig. 5 (ESI †)**. The intensity ratio of these transitions (defined as $I=I_{(5D0-7F2)}/I_{(5D0-7F1)}$) is an effective probe for monitoring the site symmetry of Eu^{3+}. It is calculated from the emission spectra and lower is this ratio; the higher is the site symmetry around europium ion. The value of ''I'' is found to be 5.3 and 7.96 for $CaMoO_4$-Eu and $SrMoO_4$-Eu respectively. The significantly higher value of I for $SrMoO_4$-Eu suggests that the Eu^{3+} ions are occupying a more distorted environment in the $SrMoO_4$ compared to $CaMoO_4$.. This is in line with point group symmetry obtained for $CaMoO_4$-Eu (D_2) which is higher than in $SrMoO_4$-Eu (C_{2v}). In distorted environment prevalent in $SrMoO_4$ magnitude of charge compensation defects or surface defects presence is more than that in $CaMoO_4$. These defects are source of non-radiative transitions and therefore PL intensity is less in $SrMoO_4$-Eu compared $CaMoO_4$-Eu as can be seen from **Figure 10** and **Fig. 5 (ESI †).**

Judd-Ofelt (JO) intensity parameters, Ω_J (J = 2, 4) calculated using Judd-Ofelt theory [63, 64] provide information about local environment and bonding in the proximity of lanthanide ion. Ω_2 generally known as short range parameter gives the measure of degree of covalency and polarizability of the chemical environment experienced by the Ln^{3+} ion while Ω_4 called as long range parameters is related to the bulk measurable such as viscosity and rigidity of the inorganic matrices. [11]. The application of JO theory to the quantitative analysis of Eu^{3+} emissive properties in matrix is nicely presented by Werts et al. [65], and also by our group [11, 16] and can be summarized as follow. There is a close relationship between radiative emission rates and integral PL intensity for transition between two manifolds $^5D_0$ and ^7F_J (J = 2, 4) can be written as:

$$A_{0-J} = A_{0-1}\frac{I_{0-J}}{I_{0-1}}\frac{h\nu_{0-1}}{h\nu_{0-J}} \quad (2)$$

Where I_{0-J} and I_{0-1} are integral intensities for $^5D_0 \rightarrow {}^7F_J$ and $^5D_0 \rightarrow {}^7F_1$ (pure magnetic dipole) transitions and $h\nu_{0-J}$ and $h\nu_{0-1}$ are their energies (in cm^{-1}), respectively. Since $^5D_0 \rightarrow {}^7F_1$ transition which is known as magnetic dipole transitions is not affected much by environmental effect its transition rate is constant with the approximate value of 50 sec^{-1} [66]. The $^5D_0 \rightarrow {}^7F_J$ (J = 2, 4, and 6) transitions are an electric dipole transition and can be expressed as follow:

$$A_{0-J} = \frac{64\pi^4 e^2 k^3}{3h(2J+1)}\frac{n(n^2+2)^2}{9}\sum_{\lambda=2,4,6}\Omega_\lambda \langle \Psi J \| U^\lambda \| \Psi' J' \rangle^2 \quad (3)$$

Where n is the refractive index of the medium, e is the electric charge, k is the transition energy of electric dipole transitions in cm^{-1}, Ω_λ is the J-O intensity parameter, and $\langle \Psi J \| U^\lambda \| \Psi' J' \rangle^2$ values are the squared reduced matrix elements, whose values are 0.0032 and 0.0023 for J' =2 and 4, respectively . Emission quantum efficiency of the emitting $^5D_0$ level is written as:

$$\eta = \frac{A_R}{A_R + A_{NR}} = \tau \sum_{J=1-4} A_J \quad (4)$$

Where the A_R rate was obtained by summing over the radiative rates for each $^5D_0 \rightarrow {}^7F_J$ (J = 1-4). The JO parameter and other photophysical values are mentioned in **Table 2**.

The most interesting observation is that for $CaMoO_4$-Eu; Ω4 value is greater than Ω_2 indicating the existence of low covalency between Eu^{3+} and ligand and relatively symmetric environment around europium ion in $CaMoO_4$ which is highly probable because it occupies Ca^{2+} (ionic size proximity). This is also reflected in the lower asymmetric value compared to $SrMoO_4$-Eu. On the other hand for $SrMoO_4$-Eu; it is other way around i.e. Ω_2 value is greater than Ω_4 indicating high covalency and low symmetry around europium ion which is the case

also as seen in point group symmetry (C_{2v}) and asymmetry ratio (7.96) values. Also the Ω_2 value for $SrMoO_4$-Eu is higher than in $CaMoO_4$-Eu; this itself is an indication of highly asymmetric environment of europium ion in $SrMoO_4$ compared to $CaMoO_4$. As discussed earlier that non-radiative relaxation pathways with will be more prevalent in $SrMoO_4$-Eu compared to $CaMoO_4$-Eu; radiative transition rate is higher in $CaMoO_4$-Eu sample. This together with high intensity europium ion in $CaMoO_4$ are also reflected in its high quantum efficiency.

Table 2: Photophysical properties Eu^{3+} doped CMO and SMO

System	A_{RAD} (s^{-1})	A_{NRAD} (s^{-1})	η (%)	Ω_2 (10^{-20} cm^2)	Ω_4 (10^{-20} cm^2)
$CaMoO_4$-Eu	658	1105	37.3	3.48	8.97
$SrMoO_4$-Eu	549	1305	29.6	5.92	3.25

3.8. Conclusion:

Scheelite structured $CaMoO_4$ and $SrMoO_4$ undoped and europium doped is synthesized using complex polymerization techniques and characterized using XRD. $CaMoO_4$ display a broad band at around 420 nm (blue region) whereas those of $SrMoO_4$ shows a broad band at 540 nm (Green region) on UV excitation which are attributed to charge transfer transition within MoO_4^{2-} group. Excitation spectrum of europium doped sample shows that O-Eu charge transfer peak in $CaMoO_4$ is slightly red shifted relative to $SrMoO_4$. Rather unusual observation is seen in emission spectrum where it was observed that molybdate to europium ion energy transfer is more efficient in SrMoO4:Eu compared to $CaMoO_4$:Eu. This also get's depicted in lifetime measurement where biexponential behavior is observed for $CaMoO_4$: Eu system whereas monoexponential behavior is observed for $SrMoO_4$:Eu. DFT calculations shows that Eu^{3+} ions interact strongly with $SrMoO_4$ compared to $CaMoO_4$ hence optical energy transfer from host to dopant atom is favorable in $SrMoO_4$ compared to $CaMoO_4$. XPS also shows that Mo binding energy ratio value for $^3d_{5/2}$ to $^3d_{3/2}$ does not changes at all on europium doping in case of $SrMoO_4$:Eu; making Host-dopant ET phenomenon more feasible compared to $CaMoO_4$:Eu. It was also observed that europium doping causes more distortion

in $CaMoO_4$ lattice than in $SrMoO_4$ at same level of doping which is also reflected from point symmetry calculation for europium ion;C_{2v} in $SrMoO_4$ and D_2 in $CaMoO_4$. The most interesting observation is that for $CaMoO_4$-Eu Ω_4 value is greater than Ω_2 indicating the existence of low covalency between Eu^{3+} and ligand and relatively symmetric environment around europium ion in $CaMoO_4$ which is highly probable because it occupies Ca^{2+} (ionic size proximity). Also the Ω_2 value for SMO-Eu is higher than in CMO-Eu; this itself is an indication of highly asymmetric environment of europium ion in $SrMoO_4$ compared to $CaMoO_4$.

Refernces:

1. B. P. Singh, A. K. Parchur, R. S. Ningthoujam, A. A. Ansari, P. Singh S. B. Rai, *Dalton Trans*., 2014,**43**, 4779.
2. Y. Wang, S. Gai, C. Li, X. Zhang, N. Niu, F. He, M. Zhang, P. Yang, *J. Mater. Chem. B*, 2013, **1**, 2056.
3. P. Jena, S. K. Gupta, V. Natarajan, O. Padmaraj, N. Satyanarayana, M. Venkateswarlu, *Mater. Res. Bull*., 2015, **64**, 223.
4. H. N. Luitel, R. Chand, T. Torikai, M. Yada, T. Watari, *RSC Adv*., 2015, **5**, 17034.
5. C. Hazra, T. Samanta, A.V. Asaithambi, V. Mahalingam, *Dalton Trans*., 2014, **43**, 6623.
6. K.K. Aruna, R. Manoharan, *Int. J. Hydrogen Energy*, 2013, **38**, 12695.
7. R. Ramkumar, M. Minakshi, *Dalton Trans*., 2015, **44**, 6158.
8. S. Dutta, S. Som, S.K. Sharma, *Dalton Trans*., 2013, **42**, 9654.
9. C. Shivakumara, R. Saraf, *Opt. Mater*., 2015, **42**, 178.
10. S. K. Gupta, P. S. Ghosh, A. Arya and V. Natarajan, *RSC Adv*., 2014, **4**, 51244.
11. R. Shukla, S. K. Gupta, V. Grover, V. Natarajan, A.K. Tyagi, *Dalton Trans.* 2015, **44**,10628.
12. K. Li, Y. Zhang, X. Li, M. Shang, H. Lian, J. Lin, *Phys. Chem. Chem. Phys*., 2015, **17**, 4283.
13. R. Gupta, Santosh K. Gupta, J.S. Gamre, K.V. Lohithakshan, V. Natarajan, S.K. Aggarwal, *Eur. J. Inorg. Chem., 2015,* **2015***,* 104
14. S. K. Gupta, M.K. Bhide, S.V. Godbole, V. Natarajan, *J. Am. Ceram. Soc.*, 2014, 97, 3694
15. R. Phatak, S. K. Gupta, K. Krishnan, S.K. Sali, S.V. Godbole, A. Das , *Dalton Trans*. 2014*,* 43, 3306

16. S. K. Gupta, M. Mohapatra, V. Natarajan and S.V. Godbole, *RSC Adv*. 2013, **3**, 20046
17. S.K. Gupta, M. Mohapatra, V. Natarajan and S.V.Godbole, *J. Mater. Sci*., 2012, **47**, 3504
18. S.K. Gupta, M. Mohapatra, S. Kaity, V. Natarajan and S.V.Godbole, *J. Lumin.,* 2012, **132**, 1329
19. G. S. R. Raju, E. Pavitra, Y. H. Ko, J. Su, *J. Mater. Chem.* , 2012, **22**, 15562.
20. C. J. Mao, J. Geng , X. C. Wu and J. Jie, *J. Phys. Chem. C*, 2010, **114**, 1982.
21. X. Liu, L. Li, H. M. Noh, J. H. Jeong, K. Jang and D. S. Shin, *RSC Adv.*, 2015,**5**, 9441.
22. Q. Zhang, Z. Xia, *RSC Adv.*, 2014, **4**, 53237.
23. R.F. Guan, G.H. Hou, Q.Q. Liu, *Mater. Tech*., 2014, **29**, 152
24. A. Khanna, P.S. Dutta, *J. Solid State Chem*., 2013, **198**, 93.
25. R. Cao, K. Chen, Q. Hu, W. Li, H. Ao, C. Cao, Ti Liang, *Adv. Powder. Tech*., 2015, **26**, 500.
26. B. P. Singh, A. K. Parchur, R. S. Ningthoujam, A. A. Ansari, P. Singh S. B. Rai, *Dalton Trans*., 2014,**43**, 4770.
27. Z. Hou, R. Chai, M. Zhang, C. Zhang, P. Chong, Z. Xu, G. Li, *Langmuir*, 2009, **25**, 12340.
28. Y. Jin, J. Zhang, S. Lu, H. Zhao, X. Zhang, X.J. Wang, *J. Phys. Chem. C*, 2008, **112**, 5860.
29. S. Yan, J. Zhang, X. Zhang, S. Lu, X. Ren, Z. Nie, X. Wang, *J. Phys. Chem. C*, 2007, **111**, 13256.
30. X. Ren, Y. Zhang, Q. Li, M. Yu, *Mater. Res. Bull*., 2014, **59**, 283.
31. A. P. de A. Marquesa, D.M.A. de Meloa, C. A. Paskocimasb, P.S. Pizanic, M. R. Joyac, E. R. Leited, E. Longo, *J. Solids State Chem*. 2006, **179**, 671.
32. G. Kresse and J. Furthmueller, *Phys. Rev. B: Condens. Matter Mater. Phys*. 1996, **5**, 11169.
33. G. Kresse and J. Furthmueller, *Comput. Mater. Sci*. 1996, **6**, 15.
34. J. P. Perdew, K. Burke and M. Ernzerhof, *Phys. Rev. Lett*. 1996, **77**, 3685.
35. P. E. Blochl, Phys. Rev. B: Condens. *Matter Mater. Phys*. 1994, **50**, 17953.
36. H. J. Monkhorst and J. D. Pack, *Phys. Rev. B: Condens. Matter Mater. Phys*. 1979, **13**, 5188.

37. P. E. Blochl, O. Jepsen and O. K. Andesen, Phys. Rev. B: Condens. Matter Mater. Phys. 1994, **4**, 16223.
38. Robert M. Hazen, Larry W. Finger, and Joseph W. E. Mariathasan, *J. Phys. Chem. Solids*, 1985, **46**, 253.
39. E. Gurmen, E. Daniels, J.S. King, *J. Chem. Phys*. 1971, **55**, 1093.
40. W. Ji, R. Shen, R. Yang, G. Yu, X. Guo, L. Peng and W. Ding, *J. Mater. Chem. A*, 2014, **2**, 699.
41. H. C. Swart, I. M. Nagpure, O. M. Ntwaeaborwa, G. L. Fisher and J. J. Terblans, *Opt. Exp.* 2012, **20**, 17119.
42. C. Rath, P. Mohanty, A.C. Pandey, N.C. Mishra, *J. Phys. D: Appl. Phys. 2009,* **42,** 205101.
43. L.R. Shah, B. Ali, H. Zhu, W.G. Wang, Y.Q. Song, H.W. Zhang, S.I. Shah, J.Q. Xiao, *J. Phys.: Condens. Matter. 2009,* **21,** 486004.
44. B.P. Singh, A.K. Parchur, R.S. Ningthoujam, A.A. Ansari, P. Singh, S.B. Rai, *Dalton Trans*., 2014, **43,** 4770.
45. M. Naeem, S.K. Hasanain, M. Kobayashi, Y. Ishida, A. Fujimori, S. Buzby, S.I. Shah, *Nanotechnology*, 2006, **17,** 2675.
46. X. Liu, L. Li, H.M. Noh, S.H. Park, J.H. Jeong, H.K. Yang, D.S. Shin, *Opt. Mater*., 2015, **43**, 10.
47. K.G. Sharma, N, R. Singh, *New J. Chem*., 2013, **37**, 2784.
48. J.W. Woon, C.J. Choi, D. Kim, *Mater. Trans.*, 2011, **52**, 768.
49. J.C. Sczancoski, L.S. Cavalcante, M.R. Joya, J.A. Varela, P.S. Pizani, E. Longo, *Chem. Engg. J*., 2008, **140**, 632.
50. J. Bi, C.-H. Cui, X. Lai, F. Shi, D.-J. Gao, *Mater. Res. Bull*., 2008, **43**, 743.
51. L. Chen, Y. Gao, *Chem. Engg. J*., 2007, **131**, 181.
52. J. Liu, J. Ma, B. Lin, Y. Ren, X. Jiang, J. Tao, X. Zhu, *Ceram. Int*., 2008,**34** ,1557.
53. G. Blasse and B.C. Grabmaier, Luminescent materials (Springer-Verlag, Berlin/Heidelberg/New York, 1994), p. 233.
54. L. Lv, J. Wang, W. Wang, L. Han, *J. Alloy. Compd.* 2015, **635**, 25.
55. X.Y. Chen and G.K.J. Liu, *J. Solid State Chem*., 2005, **178**, 419.
56. S. V. Eliseevaa and J.C.G Bunzli, Chem. Soc. Rev., 2010, **39**, 189.
57. Q. Ju, Y. Liu, R. Li, L. Liu, W. Luo and X. Chen, *J. Phys. Chem. C*, 2009, **113**, 2309.
58. R. D. Shannon, *Acta Crystallogr.*, 1976, **32**, 751.

59. A.P.A. Marques, D.M.A. De Melo, E. Longo, C.A. Paskocimas, P.S. Pizani, E.R. Leite, *J. Solid State Chem*. 2005, **178**, 2346

60. E. Cavalli, F. Angiuli, P. Boutinaud, R. Mahiou, *J. Solid State Chem*. 2012, **185**, 136

61. E. Cavalli, P. Boutinaud, R. Mahiou, M. Bettinelli, P. Dorenbos, *Inorg. Chem*. 2010, **49**, 4916.

62. J.C. Sczancoski, L.S. Cavalcante, M.R. Joya, J.A. Varela, P.S. Pizani, E. Longo, *Chem. Eng. J*. 2008, **140**, 632.

63. B.R. Judd, Phys. *Rev.* **1962**,127, 750-761.

64. G.S. Ofelt, *J. Chem. Phys*. **1962**, 37, 511-521.

65. M.H.V. Werts, R.T.F. Jukes, J.W. Verhoeven, *Phys. Chem. Chem. Phys*. 2002, **4**, 1542.

66. G. F. de Sa, O. L. Malta, C. M. Donega, A. M. Simas, R. L. Longo, P. A. Santa-Cruz and E. F. da Silva, *Coord. Chem. Rev*., 2000, **196**, 165.